Highly Sensitive Biofunctionalized Mesoporous Electrospun TiO2 Nanofiber Based Interface for Biosensing

ARTICLE *in* ACS APPLIED MATERIALS & INTERFACES · JANUARY 2014

Impact Factor: 6.72 · DOI: 10.1021/am404931f · Source: PubMed

5 AUTHORS, INCLUDING:

Kunal Mondal
North Carolina State University
19 PUBLICATIONS **61** CITATIONS
SEE PROFILE

Ved Varun Agrawal
National Physical Laboratory - India
54 PUBLICATIONS **776** CITATIONS
SEE PROFILE

Bansi Malhotra
Delhi Technological University
327 PUBLICATIONS **9,424** CITATIONS
SEE PROFILE

Ashutosh Sharma IITK
Indian Institute of Technology Kanpur
336 PUBLICATIONS **7,451** CITATIONS
SEE PROFILE

ACS APPLIED MATERIALS & INTERFACES

Research Article

www.acsami.org

Highly Sensitive Biofunctionalized Mesoporous Electrospun TiO_2 Nanofiber Based Interface for Biosensing

Kunal Mondal,[†] Md. Azahar Ali,[‡] Ved V. Agrawal,[‡] Bansi D. Malhotra,*[,‡,§] and Ashutosh Sharma*[,†]

[†]Department of Chemical Engineering, Indian Institute of Technology Kanpur, Kanpur, 208016, India

[‡]Department of Science and Technology Centre on Biomolecular Electronics, Biomedical Instrumentation Section, National Physical Laboratory, New Delhi, 110012, India

[§]Department of Biotechnology, Delhi Technological University, Shahbad Daulatpur, Main Bawana Road, New Delhi, 110042, India

Supporting Information

ABSTRACT: The surface modified and aligned mesoporous anatase titania nanofiber mats (TiO_2−NF) have been fabricated by electrospinning for esterified cholesterol detection by electrochemical technique. The electrospinning and porosity of mesoporous TiO_2−NF were controlled by use of polyvinylpyrrolidone (PVP) as a sacrificial carrier polymer in the titanium isopropoxide precursor. The mesoporous TiO_2−NF of diameters ranging from 30 to 60 nm were obtained by calcination at 470 °C and partially aligned on a rotating drum collector. The functional groups such as −COOH, −CHO etc. were introduced on TiO_2−NF surface via oxygen plasma treatment making the surface hydrophilic. Cholesterol esterase (ChEt) and cholesterol oxidase (ChOx) were covalently immobilized on the plasma treated surface of NF ($cTiO_2$−NF) via *N*-ethyl-*N*0-(3-dimethylaminopropyl carbodiimide) and *N*-hydroxysuccinimide (EDC-NHS) chemistry. The high mesoporosity (~61%) of the fibrous film allowed enhanced loading of the enzyme molecules in the TiO_2−NF mat. The ChEt-ChOx/$cTiO_2$−NF-based bioelectrode was used to detect esterified cholesterol using electrochemical technique. The high aspect ratio, surface area of aligned TiO_2−NF showed excellent voltammetric and catalytic response resulting in improved detection limit (0.49 mM). The results of response studies of this biosensor show excellent sensitivity (181.6 μA/mg dL^{-1}/cm^2) and rapid detection (20 s). This proposed strategy of biomolecule detection is thus a promising platform for the development of miniaturized device for biosensing applications.

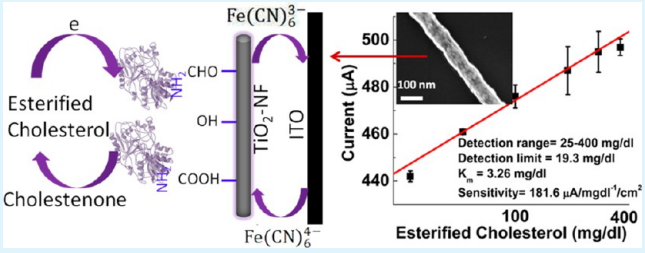

KEYWORDS: *mesoporous titania nanofibers, oxygen plasma, cholesterol detection, enzyme, electrochemical technique*

1. INTRODUCTION

There is intense interest in the application of one dimensional (1D) materials such as nanowires, nanofibers, nanotubes, etc., for the development of medical diagnostics devices.[1−6] This is because 1D nanomaterials can facilitate the fast mass transfer to and from a molecular recognition event along the entire wire resulting in significant gain in the sensing signal.[7−9] In particular, aligned 1D nanofibers may play important role in an electrochemical sensor device because of its electrocatalytic activity, mechanical strength and excellent electron transfer properties resulting in higher diffusion of redox species.[10,11] It has been found that the 1D structure can provide faster electron transport as compared to a nanopartilcles-based film of the same material.[12] The nanostrutured titania (TiO_2) has found applications in tissue engineering and drug delivery, membranes, filters, solar cells, and biosensors because of its high specific surface area, structural uniformity, chemical stability, and excellent biocompatibility.[7,13−15] However, the use of TiO_2 nanofibers as biosensing platforms has been limited to a few analytes (glucose and urea)[13,16] with a rather moderate performance owing to the low isoelectric point (~5.5) of TiO_2, which prevents stable attachment of biomolecules for functionalization. In this work, we fabricate an ultrasensitive, rapid detection, stable biosensing platform based on electrospun mesoporous aligned anatase TiO_2 nanofiber (30−60 nm) mats with hydrophilic surfaces containing −COOH, −CO, etc., which allow covalent grafting of the sensing biomolecules. In particular, we demonstrate the efficacy of this platform for the sensing of esterified cholesterol, with the results that are comparable to or exceed some of the critical performance matrices achievable by the use of other nanomaterials based platforms.

The 1D nanostrutured titania such as nanobelts and nanotubes have excellent electrochemical performances.[17,18] Interestingly, TiO_2 nanofibers have found several interesting applications requiring efficient charge transfer, large surface area, and chemical stability.[19,20] Kim et al. have reported an ultrasensitive chemiresistor using electrospun TiO_2 nanofibers (TiO_2−NF).[10] Lee et al. used electrospun TiO_2 nanorod photoelectrodes to

Received: November 5, 2013
Accepted: January 21, 2014
Published: January 21, 2014

   dx.doi.org/10.1021/am404931f | *ACS Appl. Mater. Interfaces* 2014, 6, 2516−2527

investigate charge transport characteristics of high efficiency dye-sensitized solar cells.[21] Yu et al. reported a crystalline mesoporous TiO_2 that shows high photocatalytic activity due to the synergistic effect, mesoporous structure, and crystallization.[22]

The electrospinning of TiO_2−NF is known to be a low cost and mass production technique that can be used to create electrically charged jets from polymer solutions or melts by application of an electric field (∼kilovolts).[23−26] Since electrospinning is a continuous process devoid of any contact force for elongation, very long fibers can be collected into a 3D mat.[27,28] Additionally, the electrospun TiO_2−NF may comprise of a thinner diameter and a very high surface to volume ratio further enhanced by porosity.[29] The size of TiO_2−NF can be easily controlled by tuning solution viscosity, flow rate of melt, electric field, humidity etc. The porous structure of TiO_2−NF can facilitate enhanced biomolecules adsorption and improved diffusion efficiency.[16] In this context, we have selectively removed the polymer phase from electrospun nanofibers to generate mesoporosity in the resultant nanofibers. It has been found that the electrospun nanofibers provide higher binding sites (1×10^{-7} to 2×10^{12}) to interact with biomolecules leading to higher sensitivity and detection limit.[30]

Cholesterol biosensors based on metal oxides and carbon nanotubes have been developed.[31−33] The utilization of anatase TiO_2 nanoparticles for developing microfluidic cholesterol biosensor has been recently investigated.[34] The direct attachment of biomolecules (such as enzyme, DNA, antibodies, etc.) with TiO_2 is a major problem owing to its a low isoelectric point (∼5.5).[34] The high-purity single crystal with a high percentage reactive (001) facets may perhaps lead to improved catalytic behaviour and stability.[35,36] However, the utilization of bare TiO_2 nanoparticles has been found to result in poor sensitivity and film stability.[34] The oxygen plasma treatment may perhaps play an important role via introduction of the functional groups (−COOH, −CHO, etc.) on its surface that may facilitate the covalent interaction with NH_2 group of the enzyme.[37] Additionally, the hydrophilic nature of metal oxide surface (TiO_2) is chemically compatible with enzyme molecules.[36] Tang et al. have reported chitosan modified TiO_2−NF on platinum electrode for glucose oxidase immobilization to improve electrocatalytic activity for electro-oxidation of hydrogen peroxide.[16] The higher surface area of the electrospun porous TiO_2−NF could thus provide a favorable platform for immobilization of the biomolecules resulting in good biocompatibility. The high porosity of electrospun TiO_2−NF may also allow increased adsorption of enzyme molecules. Among the various other polymorphs such as rutile, brookite, and anatase, the metastable anatase form is the most stable because of the lower average surface energy whose equilibrium crystal shape is largely dominated by the stable (101) surface.[36,38]

Cholesterol is an essential component of mammalian cell membranes, steroid hormone, cell signaling, and vitamin D.[39,40] The ratio of esterified cholesterol and free cholesterol form is 70:30 present in a human blood sample. In the bloodstream, the lipoproteins are known to carry cholesterol molecules through arteries. The free cholesterol is confined to the surface of lipoprotein particles, while the esterified cholesterol molecules are distributed to the interior. It has also been found that the high cholesterol accumulation in the blood serum is strongly correlated with coronary heart disease, arteriosclerosis, brain thrombosis, lipid metabolism dysfunction and cerebral infarction (stroke).[41] Lower level of cholesterol concentration in blood causes hyperthyroidism, anemia, malabsorption, and wasting syndrome.[42,43] Thus, the real time determination of esterified cholesterol is very crucial for clinical diagnosis.

In this study, we demonstrate an efficient cholesterol sensing platform based on mesoporous aligned anatase TiO_2−NF mat deposited on indium tin oxide (ITO) coated glass substrate. The oxygen plasma treated porous nanofiber ($cTiO_2$−NF) surface is utilized for immobilization of cholesterol esterase and cholesterol oxidase (ChEt-ChOx) molecules via strong covalent interactions. The proposed ChEt-ChOx/$cTiO_2$NF/ITO biolectrode is used to detect esterified cholesterol via electrochemical technique. Finally, we have summarized the excellent efficiency and performance of the proposed biosensor found for the esterified cholesterol measurement.

2. EXPERIMENTAL SECTION

2.1. Materials and Reagents. Titanium isopropoxide (97%), polyvinylpyrrolidone (PVP) ($M_w \approx 1\,300\,000$) were obtained from Sigma−Aldrich, U.S.A. Absolute ethanol and glacial acetic acid (99.8 %) were purchased from Merck and Fischer Scientific, India, respectively. Other chemicals including cholesterol oleate (ChOlt), cholesterol oxidase (ChOx) and cholesterol esterase (ChEt) were of analytical grade and have been purchased from Sigma Aldrich. *N*-Hydroxysuccinimide (NHS), *N*-ethyl-*N*0-(3-dimethylaminopropyl carbodiimide) (EDC) were purchased from Sigma−Aldrich (U.S.A.). Indium tin oxide (ITO) coated glass slides (film thickness ∼150−300 Å) with a resistance of 70−100 Ω/square were obtained from Vin Karola Instrument, USA. Deionized water from Millipore water systems (resistivity 18.2 MΩ.cm) was used in all experiments. The stock solutions of ChEt (1 mg dL^{-1}) and ChOx (1 mg dL^{-1}) were freshly prepared in phosphate buffer (50 mM) at pH 7.0. ChOlt solution (400 mg/dL) was first dissolved in 1% polidocanol (Brij) as a surfactant by heating/stirring resulting in clear and colourless suspension and final volume was made by addition of 0.9% NaCl solution. Further, different concentration of ChOlt have been diluted to 25−400 mg/dL using 0.9% NaCl solution.

2.2. Apparatus and Measurements. Field emission-scanning electron microscopy (FE-SEM), transmission electron microscopy (TEM), energy dispersive X-ray spectroscopy (EDX), X-ray diffraction (XRD), Raman spectroscopy, and UV−vis spectroscopy were used to characterize the synthesized TiO_2 NF. The size and morphology of the TiO_2−NF under different synthesis conditions were characterized by FE-SEM (Supra 400VP, Zeiss, Germany). The internal morphology and the phase composition of the fibers were characterized using TEM (Tecnai G^2, U.S.A.). The elemental composition of the TiO_2−NF was determined through EDX (Oxford Instruments). The XRD measurements were conducted by X'Pert Pro, PAN Analytical, Netherlands, X-ray system with Cu Kα radiation (λ = 1.54 Å) to confirm the phase of the synthesized TiO_2−NF. Raman spectral analysis was performed using WiTec, Germany, using 532 nm wavelength of laser light. UV−vis absorbance spectra of the TiO_2−NF were determined using Varian Cary 50 Bio UV−vis spectrophotometer. The pore size distribution and total surface area were measured using the Brunauer Emmett Teller (BET) method and Autosorb1 software (Quantachrome Instruments, U.S.A.). The synthesized TiO_2−NF was sonicated thoroughly in ethanol to form a homogenous solution for the absorbance measurement. The FT-IR spectral analysis of the calcined TiO_2−NF was carried out using Perkin Elmer Spectrometer, U.S.A. The electrochemical investigation was carried out using Autolab Potentiostat/Galvanostat (Model AUT-84275) in a three electrode electrochemical cell system consisting of a working electrode in phosphate buffer saline (PBS; 50 mM) containing (0.9% NaCl and 5 mM $[Fe(CN)_6]^{3-/4-}$). The Ag/AgCl acted as a reference electrode, and the platinum foil is used as a counterelectrode.

2.3. Synthesis of Mesoporous TiO_2−NF. The mesoporous TiO_2−NF were synthesized using electrospinning method.[29] Briefly, 0.45 g of polyvinylpyrrolidone (PVP) powder was added to 7.5 mL of ethanol in a capped bottle and magnetically stirred for 15 min to ensure uniform mixing. In the meantime, 1.5 g of titanium isopropoxide ($Ti(OiPr)_4$)

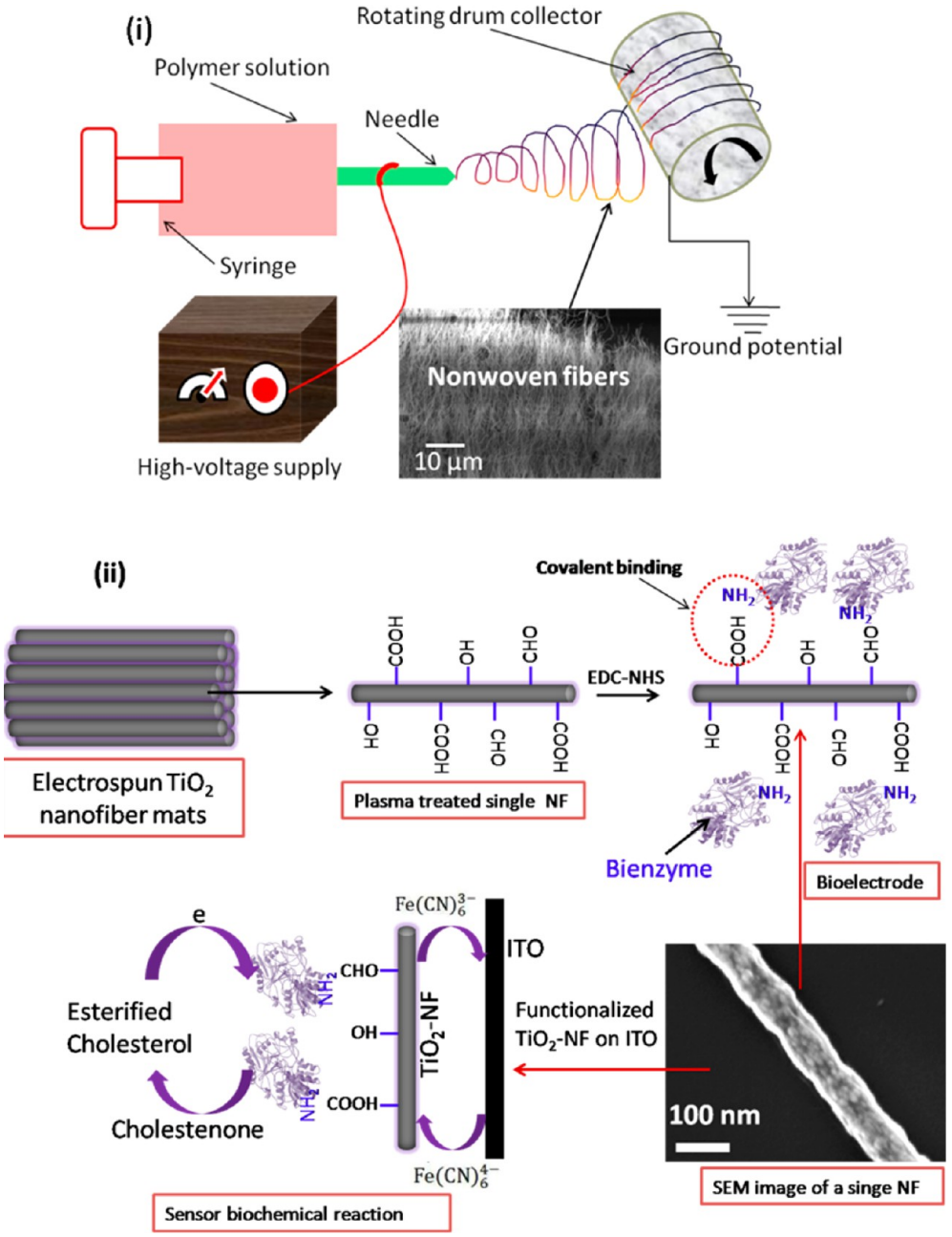

Figure 1. (i). Schematic representation of the electrospinning setup for the synthesis of aligned TiO_2 nanofibers and (ii) biofunctionalized mesoporous TiO_2−NF for esterified cholesterol detection.

was mixed with 6 mL of 1:1 mixture of ethanol and glacial acetic acid solution and stirred for 20 minutes. Then, the two mixtures were taken in a glass beaker and stirred for another 12 h at room to form a homogeneous precursor solution for electrospinning. Subsequently, this precursor solution was transferred into a plastic syringe which was connected to a high voltage DC power source by a needle tip. A stainless steel rotating drum collector wrapped allumium foil with ITO which was used as the collector for electrospun fibers (Figure 1i). The distance between the needle tip and collector was 5 cm, and 40 μL/min solution flow rate with a constant high voltage at 15 kV. The free-standing as-spun electrospun collected NF were calcined in presence of air at 470 °C for 4 h to form anatase TiO_2−NF. All the experiments were performed in a controlled environment with relative humidity of 40% and temperature of 25 °C.

2.4. Oxygen Plasma Treatment. The fabricated TiO_2−NF/ITO electrode surface was used to treat oxygen plasma. During oxygen plasma treatment, the vacuum pressure was set to 0.005 mbar, and the oxidation has been performed in low intensity mode for 0.5 h. Oxidation voltage was kept at 450 V and the continuous pure oxygen has been supplied during the plasma treatment. Oxygen plasma can remove residual organic impurities and weakly bound organic contamination on the TiO_2−NF/ITO surface. Other than enhanced surface adhesion and wettability properties, it offers ultra clean surface for biomolecules loading. The TiO_2−NF/ITO surface can create various functional groups, such as −CHO, −COOH, −OH, etc., were confirmed using FT-IR studies.

2.5. Eenzyme (ChEt-ChOx) Immobilization. For biofunctionalization, the fresh solutions of 1 mg/mL ChEt and 1 mg/mL ChOx were mixed in the ratio 1:1. A 10 μL solution of this mixture was uniformly spread onto oxygen plasma treated TiO_2−NF ($cTiO_2$−NF/ITO) surface via physical absorption and was kept in a humid chamber for 12 h at 4 °C. The available functional groups (−COOH, −CHO, and −OH) on surface of $cTiO_2$−NF/ITO film were utilized to interact with $-NH_2$ terminal of enzyme via covalent binding (amide bond) (Figure 1ii).

Prior to enzyme immobilization, the $cTiO_2$−NF/ITO surface was treated with EDC-NHS. The −COOH functional groups were activated using EDC/NHS chemistry in which EDC (0.2 M) works as a coupling agent and NHS (0.05 M) works as an activator. This ChEt-ChOx/$cTiO_2$−NF/ITO-based bioelectrode was washed with PBS (pH 7.0) to remove any unbound enzymes from the electrode surface. The bioelectrode was stored at 4 °C without exposure to the UV light when not in use. Without a long term exposure, the bioelectrode response was stable and reproducible. It has been found that the ChEt-ChOx/$cTiO_2$−NF/ITO bioelectrode shows very high catalytic behavior in phosphate buffer saline at pH 7.4 (50 mM, 0.9% NaCl) containing $[Fe(CN)_6]^{3-/4-}$ (5 mM).

3. RESULTS AND DISCUSSION

3.1. Morphological Studies. FE-SEM images of the as-spun PVP/$Ti(OiPr)_4$ composite nanofibers via electrospinning before calcination are shown in Figure 2. The $Ti(OiPr)_4$ is used as a sol−gel precursor which endures a very fast hydrolysis due to existence of moisture leading to TiO_2 gel formation in electrospun NF. The PVP acts as a carrier polymer for the $Ti(OiPr)_4$ precursor which gets detached through calcination and the residual TiO_2 retains the continuous NF morphology. Figure 2a and 2b show low and magnified images of as-spun TiO_2−NF. The key parameters of electrospinning, concentration of the solution blend (wt. %), solution flow rate and electric field strength, were varied to fabricate fibers of PVP/$(Ti(OiPr)_4)$ with diameter ranging from 165−400 nm. The electrospinning process was optimized based on the results discussed below. At a solution flow rate of 40 μL/min, the fiber diameter decreased with the decrease in the polymer concentration until a critical polymer concentration (3 wt. %) below which discrete polymer beads rather than continuous fibers were observed (results not shown). Good quality, uniform diameter fibers without beads were obtained at polymer concentration of 6 wt.%. Figure S1 (Supporting Information) shows the variation of fiber diameter with polymer weight percent. At a higher polymer concentration of 18 wt. %, thick rough fibers of 400 nm were created. With the raise in the flow rate of the 6 wt. % solution, the average fiber diameter increased as shown in the Figure S1 (Supporting Information). Thus, 40 μL/min flow rate of 6 wt. % solution was chosen. Further, electric field was also varied under these conditions. The average fiber diameter was 140 and 210 nm for 3 and 4 kV/cm, respectively. At the lower end of the electric field strength, fibers of non-uniform diameter formed at low production rate. The higher end of the range resulted in the nonuniform fiber morphology, the increased incidence of thicker the average fibers and the presence of micro-droplets on the fibers. Hence, an intermediate field strength of 3 kV/cm was chosen to yield optimally structured nanofiber web. The dense and partially aligned fiber mats used in this study were thus electrospun from a 6 wt. % PVP/$(Ti(OiPr)_4)$ solution on an ITO substrate mounted on a rotating drum. Figure 2a demonstrates structure of fibers electrospun in 6 wt. % polymer concentration and 40 μL/min solution flow rate with a steady use of 3 kV high electric potential between a tip and collector with a distance of 5 cm. Figure 3a shows FE-SEM micrograph of the synthesized unaligned TiO_2−NF (randomly oriented) derived by the calcination of electrospun TiO_2−NF. Using static collector in electrospinning results in unaligned TiO_2−NF because of instability of polymer jet or melt (Figure 3a). The free-standing TiO_2−NF scaffold is shown in image b and its high resolution image is shown in image c. Figure 3d shows the FE-SEM image of calcined TiO_2−NF prepared by electrospinning. It can be seen that TiO_2−NF are partially aligned and uniform in diameter.

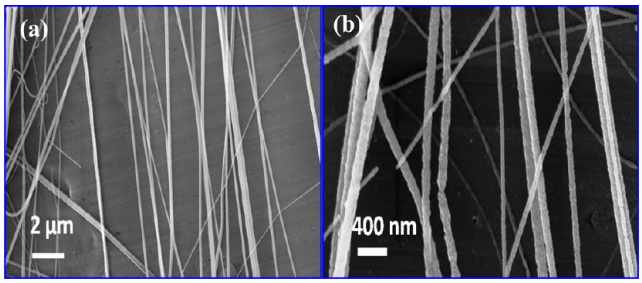

Figure 2. FE-SEM images of the as-spun PVP/$Ti(OiPr)_4$ composite nanofibers (a) lower magnification and (b) higher magnification before calcination.

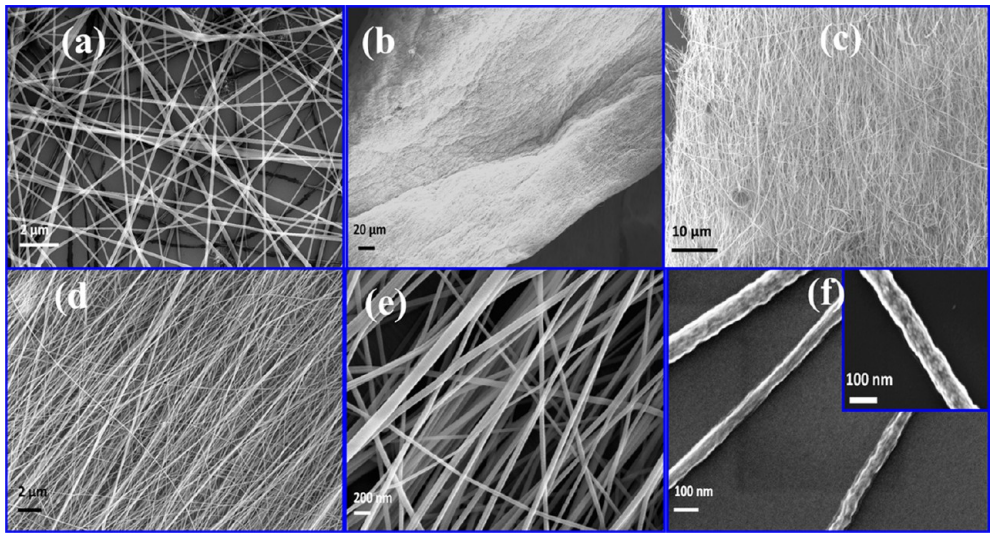

Figure 3. FE-SEM images of the electrospun TiO_2−NF after calcination (a) unaligned TiO_2−NF, (b) free standing nanofibers mat, (c) its high resolution image, and (d) lower and (e) higher magnification images of TiO_2−NF grown on ITO film. (f) FE-SEM image of dispersed TiO_2−NF, inset: individual TiO_2−NF.

dx.doi.org/10.1021/am404931f | ACS Appl. Mater. Interfaces 2014, 6, 2516−2527

From the FE-SEM analysis (Figure 3), the ratio of partially aligned TiO_2−NF is estimated to ∼83 % and the rest are randomly oriented. The high resolution image in Figure 3e shows that the TiO_2−NF are bead-free solid-shape structures. The use of rotating drum collector makes the fibers partially aligned because of the mechanical stretching of fibers during rotation of the collector. The size of the electrospun TiO_2−NF can be controlled by various factors, such as viscosity of the solution blend, solution flow rate, electric field strength, ambient properties (temperature, humidity level, etc.) that may thus play roles in the biosensing characteristics. A smaller fiber diameter and increased porosity offer increased specific surface area allowing enhanced biomolcules loading. It may be noted that the as-spun fibers when subjected to calcination at 470 °C undergoes ∼60% reduction in diameter (30−60 nm; Figure 3f). The electrospun nanofiber mats thus formed on the ITO substrate were calcined at different temperatures: 350, 470, and 600 °C (ramp rate = 8 °C/min) for 4 h. It was observed some rutile phase appears in the XRD spectra at higher calcination temperature at 600 °C, whereas higher amounts of carbon residue were left at 350 °C (data not shown). Thus, the calcination temperature was optimized at 470 °C for all the synthesized fibers to ensure carbon residue free pure anatase phase of TiO_2 −NF. Clear nanostructure of the fibers can be seen having a diameter of ∼30−60 nm. In our experiments, there was good adhesion as evidenced by the lack of physical detachment and good conductivity. Yang et al.[44] demonstrated similarly deposited electrospun TiO_2−NF mats adhere well on ITO which allows fabrication of solar cells. The individual TiO_2−NF is shown in the inset of image (Figure 3f). It appears that the TiO_2 nanoparticles perhaps assemble to form the continuous fiber structure. After enzyme functionalization (ChEt-ChOx) on $cTiO_2$−NF surface, the film surface shows transparent coating of the enzyme molecules (Figure 4a). It can be seen that these TiO_2−NF get agglomerated by incorporation of enzyme molecules. The high resolution image shows an individual TiO_2−NF wherein the enzyme molecules are attached to the pores of the nanofibers resulting in reduced pore size (Figure 4b). Thus, these TiO_2 −NF may perhaps be useful to load enzyme molecules via strong covalent interactions.

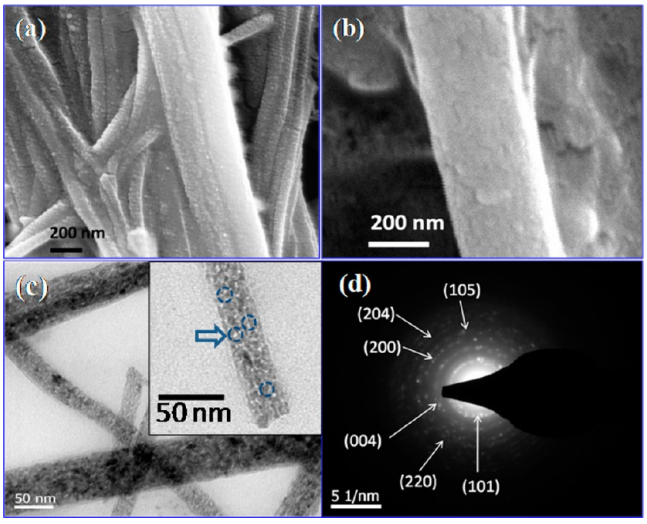

Figure 4. FE-SEM images of the ChEt/ChOx/$cTiO_2$−NF film (a) and its high resolution image (b). (c) The TEM image of electrospun TiO_2 nanofibers, and mesopores are shown in the inset, (d) SAED pattern of the TiO_2 nanofibers.

The TEM image of TiO_2−NF deposited on carbon-coated copper grid is shown in Figure 4c. It can be seen that the clear fibrous and homogeneous structures of TiO_2−NF are randomly oriented with average diameter of 70 nm. The observed TiO_2−NF diameter is in strong agreement with the FE-SEM results. In addition, TEM micrograph (inset of Figure 4c) shows that the mesopores (pore diameter ∼2−50 nm) are present in the fibers which are also corroborated by the BET studies. It is apparent that the TiO_2−NF seen by FE-SEM micrographs are made of a number of crystallites which are observed by TEM image. Selected area electron diffraction pattern (SAED) indicates that the TiO_2−NF are highly crystalline in nature resulting in improved charge transfer between electrode and the active site of enzyme (Figure 4d). The SAED pattern of the TiO_2−NF reveals the crystal planes (shown by arrow) which are also evident in the XRD studies.

The elemental confirmation of TiO_2−NF after calcination was evaluated using EDX mapping (Figure 5a). The EDX mapping confirms the presence of Ti (image b) and O_2 elements (image c) in TiO_2−NF. A small amount of carbon was also detected in EDX spectra of the TiO_2−NF (Figure 5d). The quantitative EDX analysis explains a residual carbon weight percentage of around 4% and the weight percentage of titanium and oxygen to be about 55% and 41% (shown in the inset of Figure 5d). A small amount of carbon was also detected which allows the formation of functional groups (such as −OH, C═O, C−O−C, −CHO, C−O−OH, and C═C) on its surface under the influence of oxygen plasma treatment as revealed by the results of the FTIR studies. This carbon residue thus helps in subsequent enzyme immobilization. The quantitative EDX analysis explains a residual carbon weight percentage of around 4% and the weight percentage of titanium and oxygen to be about 55% and 41% (Figure 5b). The existence of the trace amount of carbon is probably because of unfinished elimination of the PVP during calcination which may be more completely eliminated by calcination at higher temperature. However, higher calcination temperature may also lead to reduced porosity and also cause the phase transformation of anatase to rutile phase of titania which is electrochemically less active.

3.2. Structural Studies. Figure 6a shows the room temperature Raman spectra of the TiO_2−NF after heat treatment at 470 °C. The resultant spectra indicate the intensification of the lowest-frequency E_g mode. After calcination, a strong peak appears at 146 cm^{-1} at the high-frequency side of the E_g mode that is assigned to the anatase phase of TiO_2−NF.[45] Additionally, the peaks observed at around 396, 517, and 642 cm^{-1} further confirm the anatase phase of TiO_2−NF[46] and are assigned for the B_{1g}, A_{1g}, and E_g modes, respectively.

The powder X-ray diffraction (XRD) was carried out to confirm the crystal phase formation and nanocrystallite size in synthesized TiO_2−NF (Figure 6b). Various peaks of TiO_2−NF were assigned to anatase phase among different polymorph of TiO_2. In particular, the peak at $2\theta = 25.4°$ for the plane (101) was represented in the anatase phase. The peaks found at 2θ = 25.30, 36.96, 37.82, 48.04, 53.88, 55.06, 62.68, 68.76, 70.28, 75.04, and 82.16 represent the (*hkl*) crystal planes for (101), (103), (004), (200), (105), (211), (204), (116), (220), (215), and (224), respectively. The dominant peak found at 2θ = 25.4° corresponding to (101) planes of anatase TiO_2 indicates the growth of TiO_2 grains along the (101) direction. All the XRD peaks were matched with Pearson's Crystal Data (PCD) (File

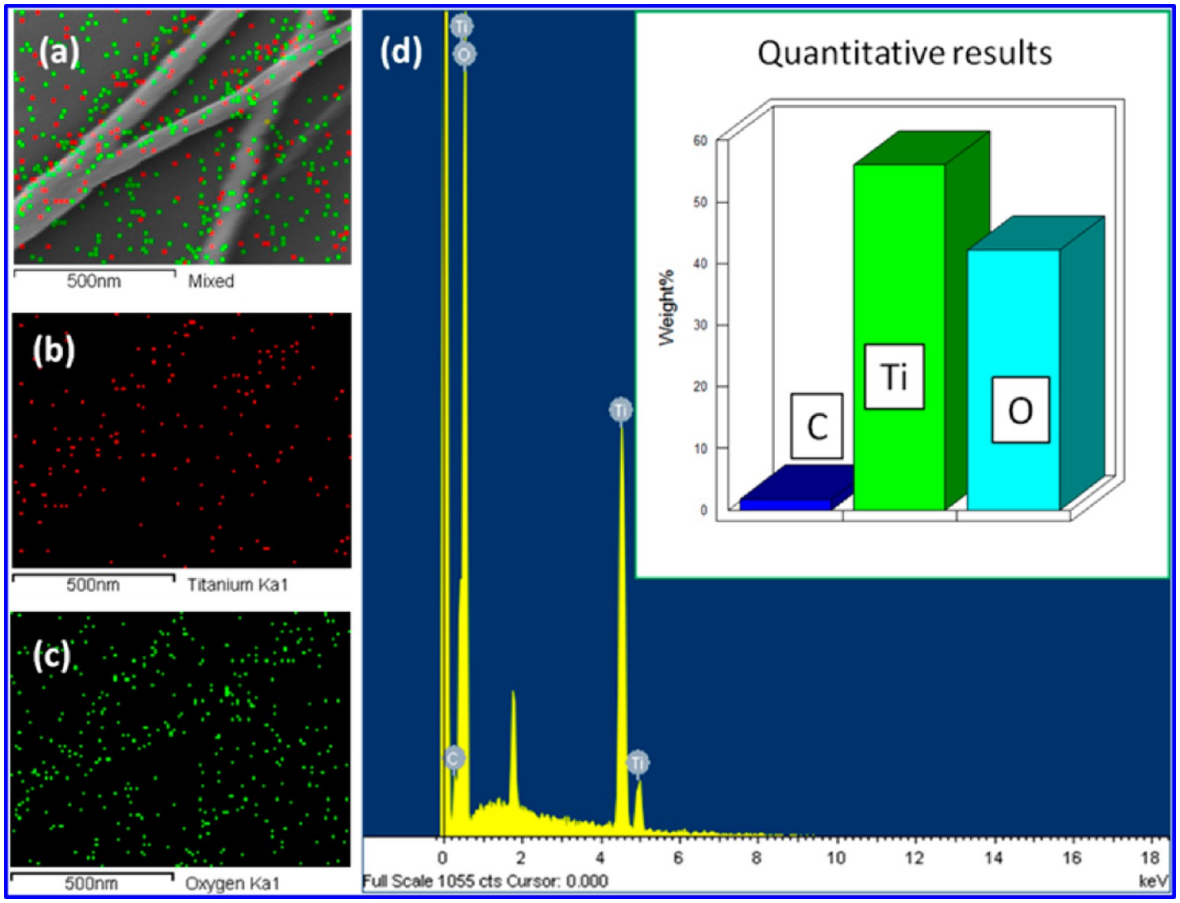

Figure 5. EDX mapping of electrospun TiO_2 nanofibers: (a) mixed (Ti and O), (b) titanium, and (c) oxygen. (d) EDX spectra and quantitative composition of TiO_2 nanofibers calcined at 470 °C.

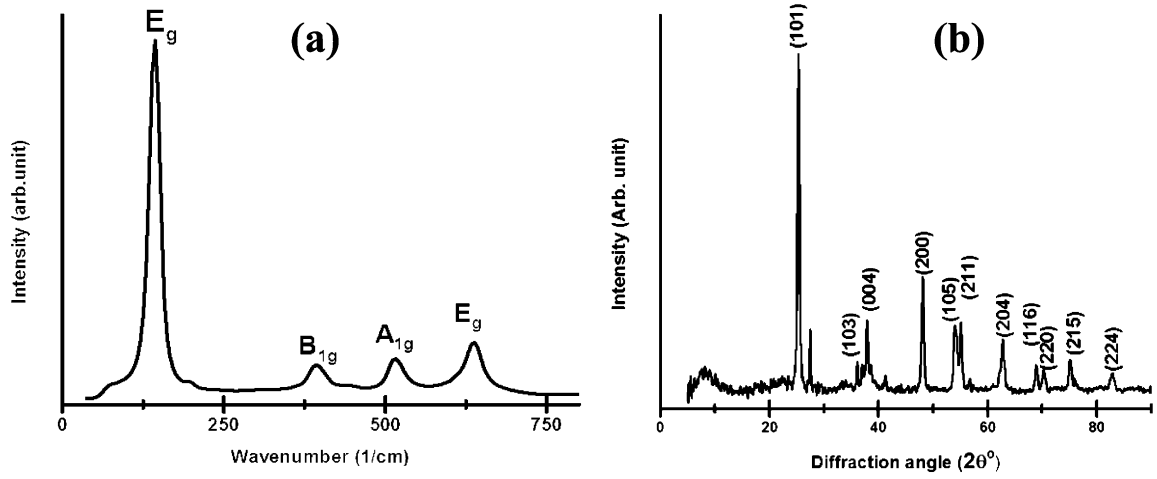

Figure 6. (a) Raman spectra of TiO_2−NF(calcined at 470 °C) at room temperature and (b) XRD analysis of the TiO_2−NF.

number 1218279). The nanocrystallite size of anatase TiO_2−NF can be calculated from the broadening of corresponding X-ray diffraction peak (101) by Scherrer's formula[47] (eq 1):

$$L = \frac{Kl}{\beta \cos \theta} \tag{1}$$

where L is the crystallite size, l is the wavelength of the X-ray radiation, K is usually taken as 0.94, known as Brags constant and β is the line width at half maximum height, after subtraction of equipment broadening. Crystallite size (L) of the TiO_2−NF by means of the Scherrer equation is calculated as ∼28.8 nm. This shows that one fiber grain is approximately three to four crystallites in electrospinning derived NF which are also supported by FE-SEM and TEM studies. The optical absorbance coefficient α of TiO_2−NF close to its band edge can be articulated by the eq 2

$$\alpha = \mathrm{A}(h\nu - E_g)^n / h\nu \tag{2}$$

where α is the absorption coefficient, $h\nu$ is the photon energy (h and ν are the Planck constant and frequency), E_g is the optical

dx.doi.org/10.1021/am404931f | ACS Appl. Mater. Interfaces 2014, 6, 2516−2527

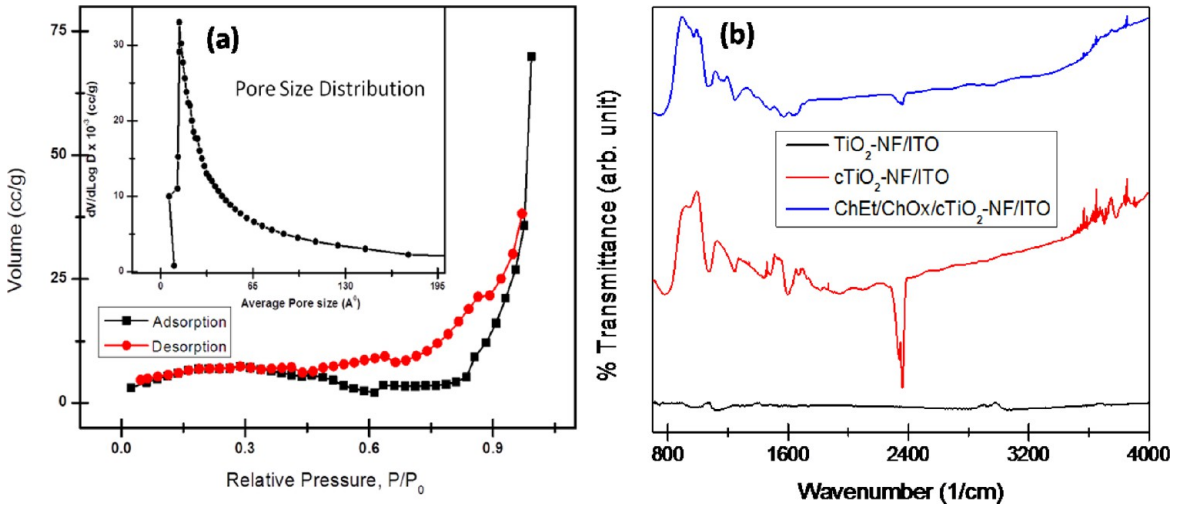

Figure 7. (a) Nitrogen adsorption/desorption isotherm of the TiO_2 nanofibers. Inset: Pore size distribution plot. (b) FT-IR spectra of the oxygen plasma treated (red curve) and bare electrospun TiO_2 nanofibers (black curve).

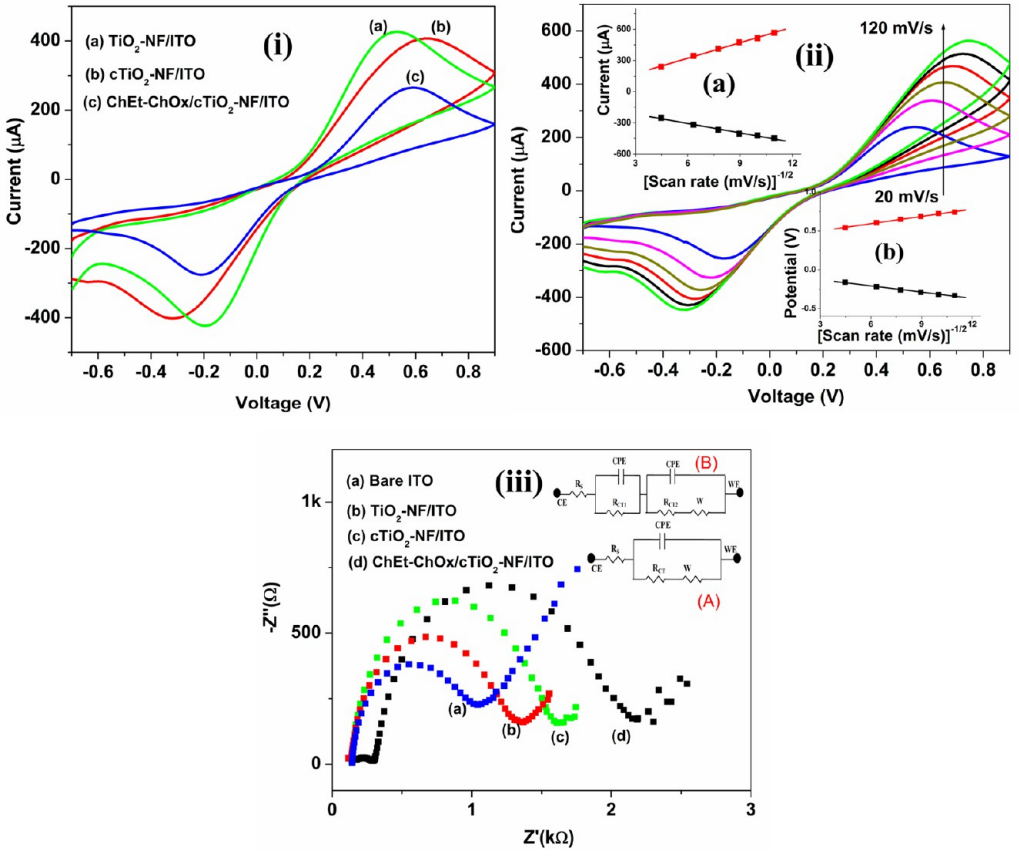

Figure 8. (i) Cyclic voltammetry (CV) studies of various fabricated electrodes at a scan rate of 20 mV s^{-1} and (ii) CV studies of ChEt-ChOx/$cTiO_2$–NF/ITO bioelectrode as a function of scan rate [20–120 mV/s]. Inset a: Anodic peak current versus root mean square of scan rate plot. Inset b: Peak potential versus root mean square of scan rate plot. (iii) Electrochemical impedance spectroscopy (EIS) studies of various fabricated electrodes. Inset: (A) The Randles equivalent circuit of the EIS spectra for the electrodes a, b, and c, and (B) the Randles equivalent circuit of the EIS spectra for the electrode d.

band gap, A is constant, and $n = 2$ related to indirect allowed transition.[48] Figure S2 (Supporting Information) shows the absorption spectra of TiO_2–NF. The absorption band edge was found to be around 372 nm (about 3.35 eV) wavelength region. The band gap energy of TiO_2 can be estimated by extrapolation to the zero coefficient, which was calculated from eq 2. The indirect band gap was estimated using Tauc plot shown in the inset of Supporting Information Figure S1. The band gap (E_g) of synthesized TiO_2–NF (3.35 eV) is higher than 3.2 eV as compared to that of the bulk TiO_2. A blue shift of 0.15 eV has been observed in the synthesized TiO_2–NF owing to smaller diameter of the fibers compared to that of bulk TiO_2 material.

dx.doi.org/10.1021/am404931f | ACS Appl. Mater. Interfaces 2014, 6, 2516–2527

The mechanisms involving phonon confinement and surface strain has been proposed to explain the blue shift and broadening of the E_g Raman mode in TiO_2 nanoparticles.[45] No photon confinement effect is observed in the main TiO_2 anatase peak at 146 cm^{-1} as the fiber diameter (30−60 nm) is large compared to the size where confinement becomes important (<15 nm). Thus, the mechanism related to the surface strain appears likely.

The higher band gap may be due to the enhancement of crystallinity of anatase phase calcined at high temperature ∼470°C. The value of band gap (TiO_2−NF; 3.35 eV) validates the crystallite size that obtained in XRD studies (28.8 nm) which is less as compared to that of bulk TiO_2 (3.2 eV).

For quantifying the specific surface area, the calcined TiO_2−NF were degassed in vacuum at 200 °C for 8 h.The nitrogen adsorption and desorption isotherms were obtained (Figure 7a). The pore size distribution was calculated by means of non-local density functional theory (NLDFT) from the adsorption branch of the isotherm. The total volume was evaluated from the adsorbed N_2 gas at relative pressure (P/P_0) of 0.99286. The total BET surface area was found to be 21.69 m^2/g with an average pore diameter of 19.98 nm, whereas the pore volume was found to be 0.1083 cc/g. The mesopore, macropore, and micropore volume were calculated as 0.065 cc/g, 0.037, and 0.005 cc/g, respectively. Thus, the pore size distribution indicates a ∼61% mesopores mixture with ∼34% macropores and ∼5% micropores. Pore size distribution curve along with the isotherm has been shown in Figure 7(a, inset).

Figure 7b shows FTIR spectra of the surface modified TiO_2−NF before and after using oxygen plasma treatment. The peak found in the finger print region (500−1000 cm^{-1}) is assigned to the O−Ti−O vibration bend (both curve). An absorption peak seen at 1200 cm^{-1} was attributed to the bicarbonate HCO_3 stretching because of CO_2 absorption of film surface (both curve). The Ti−OH wide absorption peak (red curve) was detected at 3275 cm^{-1}. The strong absorption peak seen at 1049.5 cm^{-1} reveals presence of the Ti−O−C group in the TiO_2−NF. The characteristic peak of O−H group at 3542.3 cm^{-1} found in the spectrum corresponds to the hydrogen bond among the TiO_2 molecules.[49] The broad band seen at about 3000−4000 cm^{-1}, allotted to OH vibration is shown both on plasma untreated and treated TiO_2 NF. In the FTIR spectra of plasma treated TiO_2−NF, a new peak seen at 1722 cm^{-1} can be allocated to C═O stretching vibration.[50] Another peak was also noticed in the spectra of plasma treated TiO_2−NF at the wave number of 1324 cm^{-1}, which can be a characteristic to the OH deforming bond vibration. A band at 1123 cm^{-1} can be assigned to C−O stretching vibration.[51] A strong peak seen at 1600 cm^{-1} reveals the presence of the carboxyl group on TiO_2−NF due to oxygen plasma treatment. The FTIR results indicate that the surface of plasma treated TiO_2−NF is a modified surface which holds organic functional groups, such as −COOH, C═O, and $-CH_2-$.

3.3. Electrochemical Studies. Figure 8i shows the cyclic voltammograms (CVs) obtained for TiO_2−NF/ITO (a), $cTiO_2$−NF/ITO (b), and ChEt-ChOx/$cTiO_2$−NF/ITO bioelectrodes. It has been observed that all CVs show well-defined redox properties. The peak-to-peak voltage (ΔE) of fabricated TiO_2−NF/ITO electrode [curve, a] was found to be 0.7 V, while the ΔE was estimated as 0.9 V for $cTiO_2$−NF/ITO electrode. The lower ΔE can be attributed to the fast electron transfer of $[Fe(CN)_6]^{3-/4-}$ species towards the electrode. The presence of various functional groups (OH, COOH, C═O, etc.) in oxygen plasma treated TiO_2−NF surface may somewhat hinder electron transfer resulting in slightly decreased current (0.41 mA) compared to that of TiO_2−NF/ITO electrode (0.43 mA). In addition, TiO_2−NF can act as mediators for oxidation/reduction between electrode and bulk solution followed by a conduction channel resulting in enhanced current. After incorporation of enzymes (ChEt-ChOx) on the mesoporous structure of $cTiO_2$-NF surface, the magnitude of current is found to decrease because of inherent insulating nature of enzyme which acts as a barrier for electron transport. On the other hand, the mesoporous structure (pore diameter = 2−50 nm) of $cTiO_2$-NF transducer surface offers a suitable three dimensional platform for enzyme attachment. Further, the electrochemical active area (A_{ec}) of the $cTiO_2$−NF/ITO electrode (0.97 cm^2) has been changed by enzyme functionalization (0.86 cm^2).

The CV studies were conducted for the ChEt-ChOx/$cTiO_2$−NF/ITO bioelectrode as a function of scan rate in the range of 20−120 mV/s (Figure 8ii). Anodic and cathodic peaks current/potential vary proportionally with square root of scan rate (eqs 3 and 4) and peak potential (eqs 5 and 6) shifts towards higher value indicating diffusion controlled process (inset, Figure 8ii). It has been seen that the redox peak potential shifts (anodic peak potential towards positive potential side and cathodic peak potential towards negative potential side) as the scan rate increases from 20 to 120 mV/s. The value of ΔE_p increases as the sweep rate is increased, disclosing that electron transfer kinetics has a quasi-reversible behavior. The proportional increase in the anodic and cathodic peak potentials as a function of square root of scan rate indicates that the electrochemical reaction is a diffusion controlled process.

$$I_a = 2.43 \times 10^{-5}A + 4.96 \times 10^{-5}A/[\text{mV/s}]^{1/2} \times [\text{scan rate (mV/s)}]^{-1/2} \quad R^2 = 0.998 \tag{3}$$

$$I_p = -1.24 \times 10^{-4}A - 3.01 \times 10^{-5}A/[\text{mV/s}]^{1/2} \times [\text{scan rate (mV/s)}]^{-1/2} \quad R^2 = 0.994 \tag{4}$$

$$V_a = 0.405V + 0.031V/[\text{mV/s}]^{1/2} \times [\text{scan rate (mV/s)}]^{-1/2} \quad R^2 = 0.997 \tag{5}$$

$$V_p = -0.464 - 0.026V/[\text{mV/s}]^{1/2} \times [\text{scan rate (mV/s)}]^{-1/2} \quad R^2 = 0.995 \tag{6}$$

The surface concentration for the $cTiO_2$−NF/ITO and ChEt-ChOx/$cTiO_2$−NF/ITO bioelectrodes were calculated using eq 7

$$\Gamma = \frac{Q}{nFA_{ec}} \tag{7}$$

where Γ is the number of mol/cm^2, Q is the charge obtained by integrating the anodic peak, n is the number of electrons involved in the reaction, and F is Faraday's constant. It is found that the surface concentration for ChEt-ChOx/$cTiO_2$−NF/ITO bioelectrode is 8.83 × 10^{-8} mol/cm^2 compared to the lower concentration (6.8 × 10^{-8} mol/cm^2) for the $cTiO_2$−NF/ITO electrode. This indicates that the ChEt-ChOx molecules interact strongly with the $cTiO_2$−NF matrix surface. The magnitude of diffusion coefficient (cm^2/s) of the various electrodes has been calculated using Randles-Sevcik equation.[22] It has been observed that diffusion co-efficient for ChEt-ChOx/$cTiO_2$−NF/ITO bioelectrode (31.3 $\mu cm^2/s$) is low as compared to that of the

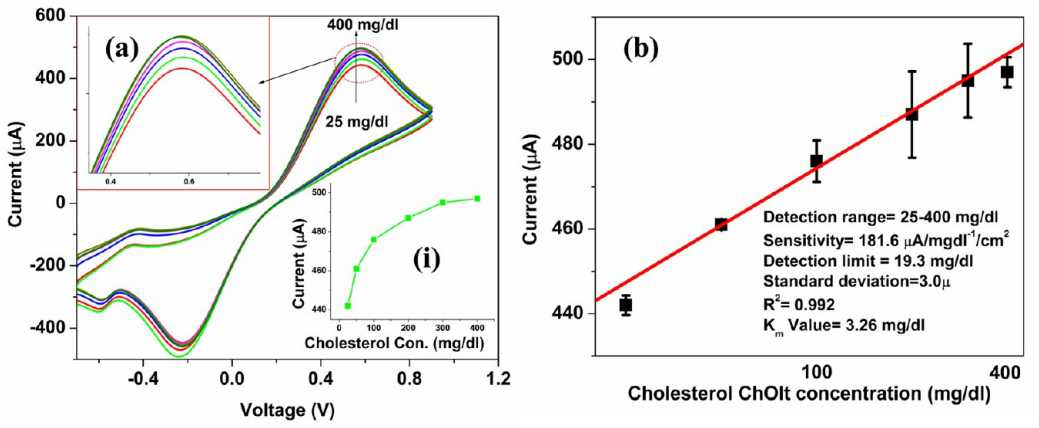

Figure 9. (a) Cyclic voltammetric response studies of the ChEt-ChOx/cTiO$_2$−NF/ITO bioelectrode as a function of cholesterol oleate concentration [25−500 mg/dL]. Inset: Zoom image anodic peak response. Inset i: Electrochemical current vs cholesterol oleate concentration plot. (b) Electrochemical current vs logarithm of cholesterol ChOlt concentration plot.

Table 1. Summary of Sensing Characteristics of the cTiO$_2$−NF Based Biosensor along with Those Reported in Literature

working electrode	detection range (mg/dL)	lower detection limit (mg/dL)	sensitivity (μA/(mg/dL)/cm^2)	K_m value (mg/dL)	stability (days)	ref
NiO nanorods	25−400	26.0	3.07	6.4	90	Ali et al[39]
anatase TiO$_2$	25−400	48.0	2.43	5.6	35	Ali et al[34]
cobalt oxide	up to 2.0	0.168	1.11	19.6		Salimi et al[53]
Au wire	4×10^{-2}−24×10^{-1}		0.021	280.0	50	Aravamudhan et al[54]
MWCNT-Au	up to 240	8.0	0.014	286.8	120	Guo et al[55]
ZnO nanoparticles	40×10^{-6}−2.0×10^{-2}	1.48×10^{-5}	0.0086	188.0	90	Umar et al[42]
electrospun TiO$_2$−NF	25−400	19.3	181.6	3.26	120	Present work

other electrodes such as cTiO$_2$−NF/ITO (74.5 μcm^2/s and TiO$_2$−NF/ITO (80.8 μcm^2/s).

3.4. Electrochemical Impedance Spectroscopy (EIS) Studies. EIS studies provide an effective method to obtain Faradic impedance between electrode and electrolyte interface. Figure 8iii shows the Nyquist plots obtained for different electrodes in the frequency range 0.01−10^5 Hz (0.01 V potential). The semicircle diameter of EIS spectra gives a value of charge transfer resistance (R_{CT}) in the higher frequency range that reveals electron transfer kinetics of the redox probe at the electrode interface. In the plot, a linear straight line at 45° to the real axis (Z') at lower frequencies indicates the diffusion limited transfer process. The R_{CT} value of an electrode depends on dielectric characteristics of the electrode/electrolyte interface. The R_{CT} value of the electrospun TiO$_2$−NF/ITO electrode (curve a, 1.11 kΩ) is found to increase as compared to that of ITO electrode (curve a, 1.0 kΩ). This may be due to the semiconducting properties of TiO$_2$−NF grown on ITO electrode. After the oxygen plasma treatment, this electrode (TiO$_2$−NF/ITO) provides higher R_{CT} value (curve c, 1.38 kΩ). However, after enzyme attachment on the surface of the cTiO$_2$−NF/ITO electrode, the R_{CT} value was again found to increase (curve d, 1.61 kΩ). The constant phase element (CPE) or double layer capacitance of cTiO$_2$−NF/ITO electrode increases to the value of 9.0μF as compared to that of the bare TiO$_2$−NF/ITO electrode. The CPE value is found to decrease for the ChEt-ChOx/cTiO$_2$−NF/ITO bioelectrode as compared to that of the other electrodes. Thus, these results confirm the enzyme functionalization on cTiO$_2$−NF surface. The corresponding Bode plots in EIS measurement for various electrodes are shown in Figure S3 (Supporting Information).

The ChEt-ChOx/cTiO$_2$−NF/ITO bioelectrode has been characterized by analyzing the following important parameters such as heterogeneous electron transfer rate constant (k_0) and time constant (τ) for redox probe containing $[Fe(CN)_6]^{3-/4-}$ ions. These studies allow interfacial interaction of biomolecules as well as help in the characterization of the structural features of the sensing interface and for explaining the mechanisms of chemical processes occurring at the electrode/solution interfaces. The corresponding k_0 of the modified electrode has been calculated by using charge transfer kinetics:

$$k_0 = \frac{RT}{n^2F^2A_{ec}R_{ct}C} \quad (8)$$

where R is the gas constant, T is the temperature, n is the electron transferring constant of the redox couple, F is Faraday constant, A_{ec} is the effective area of the electrode, and C is the concentration of the redox couple in the bulk solution. The k_0 value of the ChEt-ChOx/cTiO$_2$−NF/ITO bioelectrode (2.56 $\times 10^{-12}$/s) is higher than that for cTiO$_2$−NF/ITO electrode (2.6$\times 10^{-12}$/s), indicating a faster electron exchange between the redox species. The ChEt-ChOx immobilization on cTiO$_2$−NF/ITO shows a sluggish electron charge transfer rate constant resulting in the generation of low capacitance at the electrode surface. The observed lower value of time constant (τ) for the ChEt-ChOx/cTiO$_2$−NF/ITO bioelectrode (11.65 $\times 10^{-3}$) as compared to that of the cTiO$_2$−NF/ITO electrode 12.42 $\times 10^{-3}$ is perhaps due to the slow diffusion of $[Fe(CN)_6]^{3-/4-}$ ions at the electrode enzyme layer/solution interface.

3.5. Electrochemical Response Studies. The cyclic voltammetric response of the ChEt-ChOx/cTiO$_2$−NF/ITO

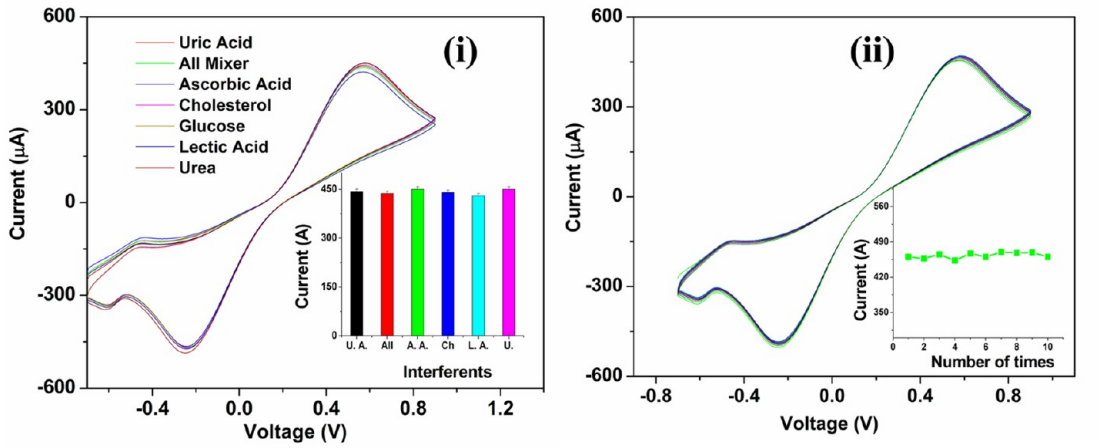

Figure 10. (i) Selectivity studies of the ChEt-ChOx/cTiO$_2$−NF/ITO bioelectrode in presence of interferents electrodes and (ii) reproducibility stability of the ChEt-ChOx/cTiO$_2$−NF/ITO bioelectrode. Inset: Current response in repeated use of ChEt-ChOx/cTiO$_2$−NF/ITO bioelectrode.

bioelectrode has been carried out with successive addition of cholesterol oleate (ChOlt) (Figure 9a) concentration. The magnitude of peak current rises sharply with increasing ChOlt concentration [25−400 mg/dL]. During the enzymatic reaction, the cholesterol molecules first react with ChEt on sensor surface and produce cholesterol and fatty acids. This cholesterol again produces cholesterol-4-ene-3-one or cholestenone and H_2O_2 by reacting with ChOx. Finally, instead of mediator electrons, the TiO_2−NF directly accepts these generated electrons via re-oxidation of H_2O_2 resulting in enhanced current (Figure 1ii). Figure 9b shows the linear plot between the magnitude of current and ChOlt concentration and the linear fit of the calibration curve is followed by eq 9

$$I(A) = 3.8 \times 10^{-4}A + 4.54 \times 10^{-5}A/(\text{mg/dL})$$
$$R^2 = 0.992 \quad (9)$$

This biosensor shows a wide detection range (25−400 mg/dL) and can be used to detect blood cholesterol in the physiological condition. The ChEt-ChOx/cTiO$_2$−NF/ITO bioelectrode exhibits high sensitivity of 181.6 mA/mg dL^{-1}/cm^2 compared to those reported in literature. Ali et al.[34] have reported the sensitivity (2.4 μA/mg dL^{-1}/cm^2) of microfluidic cholesterol biosensor using anatase-TiO_2 nanoparticles (Table 1). Using oxygen plasma treated TiO_2−NF in the proposed biosensor perhaps plays an important role in enhancing the loading capacity and better stability of biomolecules resulting from their covalent immobilization. In addition, the higher sensitivity is perhaps because of the formation of TiO_2−NF that provide a conduction channel for electron transfer between bulk solution and the electrode leading to enhanced current density. A superior electrochemical performance of aligned carbon nanofibers has been observed possibly because of a more effective electron transfer from the electroanalyte to the current collector.[52] Thus, the excellent charge transfer properties of this highly crystalline TiO_2−NF provide a suitable platform for improved biosensor characteristics as compared to those of other materials (Table 1). The lower detection limit is estimated as 19.3 mg/dL (0.49 mM) using $3\sigma_b/m$ criteria, where σ_b is standard deviation and m is the slope of the curve. The value of the enzyme−substrate kinetics (Michaelis−Menten constant, k_m) has been obtained using the Lineweaver−Burk plot revealing affinity of enzyme for desired analyte (Figure S4, Supporting Information). The Lineweaver−Burk eq 10

$$\frac{I}{I_{ss}} = \frac{1}{I_{max}} + \frac{K_m^{app}}{I_{max}C} \quad (10)$$

where I_{ss} is the steady-state current after addition of the substrate, C is the bulk concentration of the substrate, and I_{max} is the maximum current measured under saturated substrate condition. It may be noted that k_m is dependent both on matrix and the method of immobilization of enzymes that in turn bring out conformational changes resulting in different values of k_m. Also, the value of k_m for the bound enzyme can be lower or higher than that of purified enzyme. We have obtained the value of k_m for the ChEt-ChOx/cTiO$_2$−NF/ITO bioelectrode as 3.26 mg/dL, which is much lower than the reported values (Table 1). The observed lower k_m value is due to the functionalized nanofibers formation of TiO_2 on transducer surface indicating high affinity for cholesterol to ChOx and ChEt onto cTiO$_2$−NF/ITO surface for faster biochemical reaction. This result can perhaps be attributed to the higher stability of biosensing electrode. The cTiO$_2$−NF based biosensor achieves 92% of the steady-state current in less than 20 s indicating fast electron exchange between the ChEt-ChOx and cTiO$_2$−NF/ITO electrode (Figure S5, Supporting Information).

3.6. Selectivity Studies. The selectivity of the TiO_2−NF based biosensor has been tested using normal concentration of various interferents such as ascorbic acid (AA), uric acid (UA), glucose (G), lactic acid (LA), urea, and all mixer present in the blood samples (Figure 10i). The current response has been monitored for the ChEt-ChOx/cTiO$_2$−NF/ITO bioelectrode in PBS containing equal amount of ChOlt (200 mg/dL) and interferents (1:1 ratio). A negligible effect was observed with all the interferents except lactic acid as evident by low relative standard deviation (RSD = 1.7%). The storage stability of ChEt-ChOx/cTiO$_2$−NF/ITO bioelectrode has been determined by measuring change in the current response at regular interval of 1 week for about 4 months. This ChEt-ChOx/cTiO$_2$−NF/ITO bioelectrode was stored at 4 °C without exposure to the UV light. Without a long term UV exposure, the bioelectrode response was stable and reproducible. It has been found that bioelectrode retains 95% response after about 3 weeks.

3.7. Reproducibility Studies. The reproducibility of the ChEt-ChOx/cTiO$_2$−NF/ITO bioelectrode has been investigated in presence of 200 mg/dL of ChOlt concentration (Figure 10ii) using CV technique. No significant change in current value was observed after using at least 10 times under similar

conditions of repeated measurements as evidenced by the low RSD of 3.19% (n = 10). After nine measurements, the current response of the ChEt-ChOx/cTiO$_2$−NF/ITO bioelectrode decreases slightly because of the denaturation of biomolecules (Figure 10ii, inset). This result indicates that the proposed bioelectrode shows good precision.

4. CONCLUSIONS

We have demonstrated the synthesis of mesoporous aligned (partially) TiO$_2$−NF grown on ITO electrode using electrospinning technique. Surface functionalization of TiO$_2$−NF by oxygen plasma treatment introduces functional groups (COOH, CHO, OH) for efficient immobilization of biomolecules such as ChEt-ChOx. This mesoporous and oxygen plasma functionalized TiO$_2$−NF mats surface followed by EDC-NHS chemistry allows a stable loading of biomolecules. In addition, the high aspect ratio of TiO$_2$−NF improved the charge transfer between electrode and bulk solution properties resulting in higher sensitivity towards the electrochemical total cholesterol detection. The titania nanofiber platform functionalized with ChEt and ChOx biomolecules was found to have good precision and reproducibility for esterified cholesterol detection. Highly crystalline, horizontally aligned TiO$_2$−NF shows enhanced voltammetric current leading to higher signal to noise ratio. Lower detection limit (0.49 mM) and wide range detection (25−400 mg/dL) of cholesterol can be attributed to the strong amide bond formation on sensor surface. Selectivity studies of the fabricated biosensor show no significant change in redox current. Thus, plasma treated, aligned, mesoporous electrospun TiO$_2$ nanofiber mat shows excellent electrochemical and catalytic behavior that, with suitable functionalization, can have potential use in other efficient electrochemical biosensors for detection of other analytes including low density lipoproteins, urea, etc. Thus, this biosensor could be useful for the development of a point-of-care diagnostics device.

■ ASSOCIATED CONTENT

Ⓢ Supporting Information

Dependence of diameter of as-spun fibers on the polymer concentration and flow rate of the PVP/(Ti(OiPr)$_4$) solution, UV−vis absorption spectra of the TiO$_2$ nanofibers, Tauc plot for the band gap calculation, Bode plots in EIS measurement for various electrodes, Lineweaver Burk plot for K_m value estimation, and chronoamperometric response of ChEt-ChOx/cTiO$_2$−NF/ITO bioelectrode in presence of cholesterol concentration (200 mg/dL). This material is available free of charge via the Internet at http://pubs.acs.org.

■ AUTHOR INFORMATION

Corresponding Authors

*E-mail: bansi.malhotra@gmail.com.
*E-mail: ashutos@iitk.ac.in.

Author Contributions

The manuscript was written through contributions of all authors. All authors have given approval to the final version of the manuscript.

Notes

The authors declare no competing financial interest.

■ ACKNOWLEDGMENTS

This work was supported by the DST Unit of Excellence on Soft Nanofabrication from the Department of Science and Technology, New Delhi, India.

■ REFERENCES

(1) Shin, J.; Choi, S.-J.; Lee, I.; Youn, D.-Y.; Park, C. O.; Lee, J.-H.; Tuller, H. L.; Kim, I.-D. Thin-Wall Assembled SnO$_2$ Fibers Functionalized by Catalytic Pt Nanoparticles and their Superior Exhaled-Breath-Sensing Properties for the Diagnosis of Diabetes. *Adv. Funct. Mater.* **2013**, *23*, 2357−2367.

(2) Vamvakaki, V.; Tsagaraki, K.; Chaniotakis, N. Carbon Nanofiber-Based Glucose Biosensor. *Anal. Chem.* **2006**, *78*, 5538−5542.

(3) Matlock-Colangelo, L.; Baeumner, A. J. Recent Progress in the Design of Nanofiber-Based Biosensing Devices. *Lab Chip* **2012**, *12*, 2612−2620.

(4) Hsu, P.-C.; Wu, H.; Carney, T. J.; McDowell, M. T.; Yang, Y.; Garnett, E. C.; Li, M.; Hu, L.; Cui, Y. Passivation Coating on Electrospun Copper Nanofibers for Stable Transparent Electrodes. *ACS Nano* **2012**, *6*, 5150−5156.

(5) Ding, B.; Wang, M.; Wang, X.; Yu, J.; Sun, G. Electrospun Nanomaterials for Ultrasensitive Sensors. *Mater. Today* **2010**, *13*, 16−27.

(6) Wu, J.-J.; Chen, Y.-R.; Liao, W.-P.; Wu, C.-T.; Chen, C.-Y. Construction of Nanocrystalline Film on Nanowire Array via Awelling Electrospun Polyvinylpyrrolidone-Hosted Nanofibers for Use in Dye-Sensitized Solar Cells. *ACS Nano* **2010**, *4*, 5679−5684.

(7) Kim, I.-D.; Rothschild, A.; Lee, B. H.; Kim, D. Y.; Jo, S. M.; Tuller, H. L. Ultrasensitive Chemiresistors Based on Electrospun TiO$_2$ Nanofibers. *Nano Lett.* **2006**, *6*, 2009−2013.

(8) Swager, T. M. The Molecular Wire Approach to Sensory Signal Amplification. *Acc. Chem. Res.* **1998**, *31*, 201−207.

(9) Yoon, H.; Jang, J. Conducting-Polymer Nanomaterials for High-Performance Sensor Applications: Issues and Challenges. *Adv. Funct. Mater.* **2009**, *19*, 1567−1576.

(10) Huang, S.; Ding, Y.; Liu, Y.; Su, L.; Filosa, R., Jr.; Lei, Y. Glucose Biosensor Using Glucose Oxidase and Electrospun Mn_2O_3-Ag Nanofibers. *Electroanalysis* **2011**, *23*, 1912−1920.

(11) Stafiniak, A.; Boratynski, B.; Baranowska-Korczy, A.; Szyszka, A.; Ramiaczek-Krasowska, M.; Prazmowska, J.; Fronc, K.; Elbaum, D.; Paszkiewicz, R.; Tłaczała, M. A Novel Electrospun ZnO Nanofibers Biosensor Fabrication. *Sens. Actuators, B* **2011**, *160*, 1413−1418.

(12) Lee, B. H.; Song, M. Y.; Jang, S.-Y.; Jo, S. M.; Kwak, S.-Y.; Kim, D. Y. Charge Transport Characteristics of High Efficiency Dye-Sensitized Solar Cells Based on Electrospun TiO$_2$ Nanorod Photoelectrodes. *J. Phys. Chem. C* **2009**, *113*, 21453−21457.

(13) Bao, S.-J.; Li, C. M.; Zang, J.-F.; Cui, X.-Q.; Qiao, Y.; Guo, J. New Nanostructured TiO$_2$ for Direct Electrochemistry and Glucose Sensor Applications. *Adv. Funct. Mater.* **2008**, *18*, 591−599.

(14) Choi, H.; Sofranko, A. C.; Dionysiou, D. D. Nanocrystalline TiO$_2$ Photocatalytic Membranes with a Hierarchical Mesoporous Multilayer Structure: Synthesis, Characterization, and Multifunction. *Adv. Funct. Mater.* **2006**, *16*, 1067−1074.

(15) Shang, M.; Wang, W.; Sun, S.; Gao, E.; Zhang, Z.; Zhang, L.; O'Hayre, R. The Design and Realization of a Large-Area Flexible Nanofiber-Based Mat for Pollutant Degradation: An Application in Photocatalysis. *Nanoscale* **2013**, *5*, 5036−5042.

(16) Tang, H.; Yan, F.; Tai, Q.; Chan, H. L. W. The Improvement of Glucose Bioelectrocatalytic Properties of Platinum Electrodes Modified with Electrospun TiO$_2$ Nanofibers. *Biosens. Bioelectron.* **2010**, *25*, 1646−1651.

(17) Liu, W.; Gao, P.; Bao, D.; Zhang, G.; Chen, Y.; Chen, G.; Wang, Y.; Wang, L.; Yang, S.; Li, G.; Sun, Y. Topotactic Conversion Route to Ultrafine Crystalline TiO$_2$ Nanotubes with Optimizable Electrochemical Performance. *RSC Adv.* **2013**, *3*, 6531−6537.

(18) Kim, D. H.; Seong, W. M.; Park, I. J.; Yoo, E.-S.; Shin, S. S.; Kim, J. S.; Jung, H. S.; Lee, S.; Hong, K. S. Anatase TiO$_2$ Nanorod-Decoration

for Highly Efficient Photoenergy Conversion. *Nanoscale* **2013**, *5*, 11725−11732.
(19) Zhang, X.; Aravindan, V.; Kumar, P. S.; Liu, H.; Sundaramurthy, J.; Ramakrishna, S.; Madhavi, S. Synthesis of TiO_2 Hollow Nanofibers by Co-axial Electrospinning and Its Superior Lithium Storage Capability in Full-Cell Assembly with Olivine Phosphate. *Nanoscale* **2013**, *5*, 5973−5980.
(20) Nam, S. H.; Shim, H.-S.; Kim, Y.-S.; Dar, M. A.; Kim, J. G.; Kim, W. B. Ag or Au Nanoparticle-Embedded One-Dimensional Composite TiO_2 Nanofibers Prepared via Electrospinning for Use in Lithium-Ion Batteries. *ACS Appl. Mater. Interfaces* **2010**, *2*, 2046−2052.
(21) Choi, S. K.; Kim, S.; Lim, S. K.; Park, H. Photocatalytic Comparison of TiO_2 Nanoparticles and Electrospun TiO_2 Nanofibers: Effects of Mesoporosity and Interparticle ChargeTransfer. *J. Phys. Chem. C* **2010**, *114*, 16475−16480.
(22) Yu, J.; Wang, G.; Cheng, B.; Zhou, M. Effects of Hydrothermal Temperature and Time on the Photocatalytic Activity and Microstructures of Bimodal Mesoporous TiO_2 Powders. *Appl. Catal., B* **2007**, *69*, 171−180.
(23) Formo, E.; Lee, E.; Campbell, D.; Xia, Y. Functionalization of Electrospun TiO_2 Nanofibers with Pt Nanoparticles and Nanowires for Catalytic Applications. *Nano Lett.* **2008**, *8*, 668−672.
(24) Kumar, A.; Jose, R.; Fujihara, K.; Wang, J.; Ramakrishna, S. Structural and Optical Properties of Electrospun TiO_2 Nanofibers. *Chem. Mater.* **2007**, *19*, 6536−6542.
(25) Song, M. Y.; Kim, D. K.; Ihn, K. J.; Jo, S.; Kim, D. Y. Electrospun TiO_2 Electrodes for Dye-Sensitized Solar Cells. *Nanotechnology* **2004**, *15*, 1861−1865.
(26) Chuangchote, S.; Jitputti, J.; Sagawa, T.; Yoshikawa, S. Photocatalytic Activity for Hydrogen Evolution of Electrospun TiO_2 Nanofibers. *ACS Appl. Mater. Interfaces* **2009**, *1*, 1140−1143.
(27) Kumbar, S. G.; James, R.; Nukavarapu, S. P.; Laurencin, C. T. Electrospun Nanofiber Scaffolds: Engineering Soft Tissues. *Biomed. Mater.* **2008**, *3*, No. 034002.
(28) Li, D.; Wang, Y.; Xia, Y. Electrospinning of Polymeric and Ceramic Nanofibers as Uniaxially Aligned Arrays. *Nano Lett.* **2003**, *3*, 1167−1171.
(29) Li, D.; Xia, Y. Fabrication of Titania Nanofibers by Electrospinning. *Nano Lett.* **2003**, *3*, 555−560.
(30) Frey, M. W.; Baeumner, A. J.; Li, D. Electrospun Nanofiber-Based Biosensor Assemblies. United States Patent Application US 2006/0260707 A1, 2006.
(31) Ansari, A. A.; Kaushik, A.; Solanki, P. R.; Malhotra, B. D. Electrochemical Cholesterol Sensor Based on Tin Oxide-Chitosan Nanobiocomposite Film. *Electroanalysis* **2009**, *21*, 965.
(32) Wisitsoraat, A.; Karuwan, C.; Wong-ek, K.; Phokharatkul, D.; Sritongkham, P.; Tuantranont, A. High Sensitivity Electrochemical Cholesterol Sensor Utilizing a Vertically Aligned Carbon Nanotube Electrode with Electropolymerized Enzyme Immobilization. *Sensors* **2009**, *9*, 8658.
(33) Gao, P.; Bao, D.; Wang, Y.; Chen, Y.; Wang, L.; Yang, S.; Chen, G.; Li, G.; Sun, Y.; Qin, W. Epitaxial Growth Route to Crystalline TiO_2 Nanobelts with Optimizable Electrochemical Performance. *ACS Appl. Mater. Interfaces* **2013**, *5*, 368−373.
(34) Ali, M. A.; Srivastava, S.; Solanki, P. R.; Agrawal, V. V.; John, R.; Malhotra, B. D. Nanostructured Anatase-Titanium Dioxide Based Platform for Application to Microfluidics Cholesterol Biosensor. *Appl. Phys. Lett.* **2012**, *101*, No. 084105.
(35) Yang, H. G.; Sun, C. H.; Qiao, S. Z.; Zou, J.; Liu, G.; Smith, S. C.; Cheng, H. M.; Lu, G. Q. Anatase TiO_2 Single Crystals with a Large Percentage of Reactive Facets. *Nature* **2008**, *453*, 638−641.
(36) Cui, J.; Sun, D.; Chen, S.; Zhou, W.; Hu, P.; Liu, H.; Huang, Z. Enhancement of Selective Determination of the Perfect Match and Mismatch of Single Nucleobases with a Biosensing Electrode Based on Surface-Coarsened Anatase TiO_2 Nanobelts. *J. Mater. Chem.* **2011**, *21*, 10633−10636.
(37) Yoo, H. S.; Kim, T. G.; Park, T. G. Surface-Functionalized Electrospun Nanofibers for Tissue Engineering and Drug Delivery. *Adv. Drug Delivery Rev.* **2009**, *61*, 1033−1042.
(38) Choi, S. Y.; Mamak, M.; Coombs, N.; Chopra, N.; Ozin, G. A. Thermally Stable Two-Dimensional Hexagonal Mesoporous Nanocrystalline Anatase, meso-nc-TiO_2: Bulk and Crack-Free Thin Film Morphologies. *Adv. Funct. Mater.* **2004**, *14*, 335−344.
(39) Ali, M. A.; Solanki, P. R.; Patel, M. K.; Dhayani, H.; Agrawal, V. V.; John, R.; Malhotra, B. D. A Highly Efficient Microfluidic Nano Biochip Based on Nanostructured Nickel Oxide. *Nanoscale* **2013**, *5*, 2883−2891.
(40) Zhu, L.; Xu, L.; Tan, L.; Tan, H.; Yang, S.; Yao, S. Direct Electrochemistry of Cholesterol Oxidase Immobilized on Gold Nanoparticles-Decorated Multiwalled Carbon Nanotubes and Cholesterol Sensing. *Talanta* **2013**, *106*, 192−199.
(41) Parlak, O.; Tiwari, A.; P.F. Turner, A.; Tiwari, A. Template-Directed Hierarchical Self-Assembly of Graphene Based Hybrid Structure for Electrochemical Biosensing. *Biosens. Bioelectron.* **2013**, *49*, 53−62.
(42) Umar, A.; Rahman, M. M.; Vaseem, M.; Hahn, Y.-B. Ultra-sensitive Cholesterol Biosensor Based on Low-Temperature Grown ZnO Nanoparticles. *Electrochem. Commun.* **2009**, *11*, 118−121.
(43) Simopoulos, A. P. Essential Fatty Acids in Health and Chronic Disease. *Am. J. Clin. Nutr.* **1999**, *70*, 560S−569S.
(44) Yang, L.; Leung, W. W.-F. Application of a Bilayer TiO_2 Nanofiber Photoanode for Optimization of Dye-Sensitized Solar Cells. *Adv. Mater.* **2011**, *23*, 4559−4562.
(45) Choi, H. C.; Jung, Y. M.; Kim, S. B. Size Effects in the Raman Spectra of TiO_2 Nanoparticles. *Vib. Spectrosc.* **2005**, *37*, 33−38.
(46) Zhang, J.; Li, M.; Feng, Z.; Chen, J.; Li, C. UV Raman Spectroscopic Study on TiO_2. I. Phase Transformation at the Surface and in the Bulk. *J. Phys. Chem. B* **2006**, *110*, 927−935.
(47) Reddy, K. M.; Manorama, S. V.; Reddy, A. R. Bandgap Studies on Anatase Titanium Dioxide Nanoparticles. *Mater. Chem. Phys.* **2002**, *78*, 239−245.
(48) Yoo, D.; Kim, I.; Kim, S.; Hahn, C. H.; Lee, C.; Cho, S. Effects of Annealing Temperature and Method on Structural and Optical Properties of TiO_2 Films Prepared by RF Magnetron Sputtering at Room Temperature. *Appl. Surf. Sci.* **2007**, *253*, 3888−3892.
(49) Yang, H. G.; Liu, G.; Qiao, S. Z.; Sun, C. H.; Jin, Y. G.; Smith, S. C.; Zou, J.; Cheng, H. M.; Lu, G. Q. M. Solvothermal Synthesis and Photoreactivity of Anatase TiO_2 Nanosheets with Dominant {001} Facets. *J. Am. Chem. Soc.* **2009**, *131*, 4078−4083.
(50) Zhu, F.; Kong, E. S.-W.; Zhang, J.; Zhang, Y. Surface Modification of TiO_2 Nanoparticles through Plasma Polymerization of Acrylic Acid. *Chem. Phys. Lett.* **2006**, *423*, 270−275.
(51) Lee, S. D.; Sarmadi, M.; Denes, E.; Shohet, J. L. Surface Modification of Polypropylene Under Argon and Oxygen-RF-Plasma Conditions. *Plasmas Polym.* **1997**, *2*, 177−198.
(52) Islam, A. B.; Tulip, F. S.; Islam, S. K.; Rahman, T.; MacArthur, K. C. A Mediator Free Amperometric Bienzymatic Glucose Biosensor Using Vertically Aligned Carbon Nanofibers (VACNFs). *IEEE Sens. J* **2011**, *11*, 2798−2804.
(53) Salimi, A.; Hallaj, R.; Soltanian, S. Fabrication of a Sensitive Cholesterol Biosensor Based on Cobalt-Oxide Nanostructures Electrodeposited onto Glassy Carbon Electrode. *Electroanalysis* **2009**, *21*, 2693−2700.
(54) Aravamudhan, S.; Ramgir, N. S.; Bhansali, S. Electrochemical Biosensor for Targeted Detection in Blood Using Aligned Au Nanowires. *Sens. Actuators, B* **2007**, *127*, 29−35.
(55) Guo, M.; Chen, J.; Li, J.; Nie, L.; Yao, S. Carbon Nanotubes-Based Amperometric Cholesterol Biosensor Fabricated through Layer-By-Layer Technique. *Electroanalysis* **2004**, *16*, 1992−1998.